JOURNAL OF GEOPHYSICAL RESEARCH, VOL. 101, NO. B8, PAGES 17,497–17,506, AUGUST 10, 1996

Morphology and physical properties of Fontainebleau sandstone via a tomographic analysis

David A. Coker[1] and Salvatore Torquato

Department of Civil Engineering and Operations Research, and Princeton Materials Institute, Princeton University, Princeton, New Jersey

John H. Dunsmuir

Exxon Research and Engineering Company, Annandale, New Jersey

Abstract. We present a study of the morphology and bulk physical properties of a Fontainebleau sandstone via an X ray tomographic analysis. Synchrotron-based X ray tomographic techniques provide us with a high-resolution (7.5 μm), three-dimensional digitized representation of the sandstone that leaves the sample intact and unaltered. To estimate a wide spectrum of bulk properties of the Fontainebleau sandstone specimen, we extract from this image a number of different correlation functions that statistically characterize the pore-space morphology and relevant pore-space length and time scales. These statistical measures are obtainable from lineal, plane, and/or volume measurements and include the porosity, specific surface, two–point and three–point probability functions, lineal–path function, chord–length distribution function, pore–size distribution function, and coarseness. The pore–size distribution function, in particular, contains a certain level of connectedness information and accordingly can only be obtained from a three-dimensional representation of the sample. Many bulk properties of the sandstone, such as the mean survival time τ (obtainable from Nuclear Magnetic Resonance relaxation studies), fluid permeability k, effective electrical and thermal conductivities, and effective elastic moduli, can be estimated using the aforementioned statistical correlation functions. Specifically, the electrical conductivity (or, equivalently, the formation factor F), mean survival time, and fluid permeability are determined using rigorous bounds. The mean survival time and fluid permeability are also found using direct simulation techniques and cross-property relations, respectively. One such cross-property relation for k depending on τ and F gives a permeability estimate that is within a factor of 2 of the experimental result.

Introduction

Interest in understanding the structure of geologic materials dates back to the work of *Darcy* [1856]. It was well known that the structure of the rock greatly affected the flow characteristics that Darcy was measuring. Because of the complexity of the problem, Darcy introduced the bulk permeability that relates the applied pressure gradient to the average velocity of the viscous fluid flowing through the medium. It is now very well established that other bulk properties of porous and other heterogeneous media (such as the conductivity and elastic moduli) are sensitive to the full three–dimensional structure of the samples. Indeed, complete characterization of the effective properties requires knowledge of an infinite set of n-point statistical correlation functions [*Beran*, 1968; *Milton*, 1987; *Torquato*, 1991]. In practice, only lower-order morphological information is obtainable either experimentally or theoretically. Using lower-order information, one can construct rigorous bounds on a variety of effective properties of heterogeneous media [*Beran*, 1968; *Milton*, 1981; *Torquato*, 1991; *Prager*, 1961; *Prager*, 1969; *Doi*, 1976; *Milton*, 1987; *Berryman and Milton*, 1985; *Rubinstein and Torquato*, 1988; *Rubinstein and Torquato*, 1989; *Torquato and Avellaneda*, 1991] that can sometimes be highly predictive.

The process of obtaining relevant morphological quantities from actual material samples has been limited by a lack of high–resolution, pore/grain–level, three-dimensional information. With recent experimental ad-

[1]Now at Department of Mathematics and Science, SUNY Institute of Technology, Utica

Paper number 96JB00811.
0148-0227/96/96JB-00811$09.00

vances in fields such as scanning and transmission electron microscopy [*Flegler*, 1993], laser scanning confocal microscopy [*Fredrich et al.*, 1995], scanning tunneling electron microscopy [*Stroscio and Kaiser*, 1992], and synchrotron-based X ray tomography [*Flannery et al.*, 1987; *Deckman et al.*, 1989; *Dunsmuir et al.*, 1991;*Kinney and Nichols*, 1992], it is possible to obtain high-resolution two- and three-dimensional microstructural phase information of a given sample. In addition, these methods are nonintrusive leaving the sample intact and unaltered,which allows complimentary studies either by any of the aforementioned techniques or through direct experimental measurement of the same sample.

As experimental or digitized data are of finite resolution, it is important to understand the relationship between the correlation function extracted from a digitized representation and the correlation function for the actual material. This relationship is exact for infinite resolution and becomes correspondingly less so at reduced resolutions. *Coker and Torquato* [1995a,b] recently studied digitized representations of the continuum model of overlapping spheres at various resolutions and volume fractions. They discovered that for certain morphological quantities, large discrepancies arose between the exact continuum results and the measured digitized analogues. In some cases the difference was as much as 20%. However, certain morphological quantities showed little or no dependence. As the digitized nature of a medium is actually realized in the boundary between the phases, quantities sensitive to this interface showed the greatest dependence. Therefore the poorer the resolution, the worse the correlation between the digitized measurement and the actual value.

We will employ the experimental data from a microtomographic study of Fontainebleau sandstone, as this allows access to high-resolution characterization of the specimen in the full three dimensions. This sample was previously studied by *Schwartz et al.* [1994]. They conducted a direct numerical simulation on fluid motion through the pore space in an attempt to predict the fluid permeability. We focus mostly on extracting morphological measures and using this information to estimate physical properties.

To estimate a wide spectrum of bulk properties of the Fontainebleau sandstone specimen, we extract from the three-dimensional image a number of different correlation functions, some of which are obtainable from lineal, plane, and/or volume measurements. The most basic and simplest quantities are the volume fraction of phase i, ϕ_i, and specific surface (the interfacial surface area per unit volume) s. These quantities are actually one-point correlation functions. For example, in the case of a statistically homogeneous system, ϕ_i is equal to the probability of finding a point in phase i. Both ϕ_i and s can be obtained from lineal, plane or volume measurements [*Underwood*, 1970]. Higher-order information that we obtain from the specimen include: two–point and three–point probability functions $S_2(\mathbf{r})$ and $S_3(\mathbf{r},\mathbf{s},\mathbf{t})$, lineal-path function $L(z)$, chord–length distribution function $p(z)$, pore–size distribution function $P(\delta)$, and coarseness C. All of these quantities are defined precisely below and are important in determining a variety of effective properties, such as the conductivity [*Beran*, 1968; *Milton*, 1981; *Torquato*, 1991; *Milton*, 1987], elastic moduli [*Milton*, 1981], nuclear magnetic resonance (NMR) time-scales [*Doi*, 1976; *Rubinstein and Torquato*, 1988], discrete free–path properties [*Ho and Streider*, 1979; *Tokunaga*, 1985] and the fluid permeability [*Doi*, 1976; *Berryman and Milton*, 1985; *Torquato*, 1986; *Rubinstein and Torquato*, 1989].

We also estimate the formation factor (or, equivalently, the effective electrical conductivity), mean survival time (obtainable from NMR relaxation experiments [*Banavar and Schwartz*, 1987; *Wilkinson et al.*, 1991; *Strange et al.*, 1993]), and the fluid permeability of the Fontainebleau specimen. This is accomplished using bounding techniques, cross-property relations, and direct computer simulations.

X Ray Tomography and Data Segmenting

Traditional methods for obtaining three-dimensional information often involve invasive techniques. These methods are undesirable because they alter the sample in such a manner that inhibits either repeated analysis or complementary analyses using different techniques. Serial sectioning, as conducted by *J.G. Berryman et al.* [e.g., 1985, 1986] and *Dullien et al.* [e.g., *Dullien*, 1979; *MacDonald et al.*, 1986; *Kwiecien et al.*, 1990] is one such technique that leaves the bulk sample permanently destroyed. In addition, the sectioning process may alter the microstructure of each analyzed slice. Computer-aided tomography (CAT) scans provide a means for noninvasive analysis, but they are limited to resolutions of $\sim$ 100 μm which is not sufficient to explore geological samples at the pore or grain level. With x-ray synchrotrons such as the National Synchrotron Light Source (NSLS) located at Brookhaven National Laboratory producing high intensity X rays with well described continuum spectra, the reality of analyzing three-dimensional samples at the pore level has been achieved since resolutions of 1 μm are possible with typical rocks and materials.

Tomographic Process

The tomographic data used in this analysis are obtained from a sample of Fontainebleau sandstone which has two highly desirable properties: the pore phase is relatively free of inter-grain contaminants such as clay, and the grain phase (consisting of primarily quartz) tends to be very homogeneous in comparison with other sandstones. The segmenting and subsequent analysis are therefore much easier, as the specimen may be treated as a two-phase material: grain (quartz) and air.

The microtomography data and reconstructed three-dimensional maps of specimen X ray opacity are collected using the scanner [*Deckman et al.*, 1989; *Dunsmuir et al.*, 1991], located at beamline X2-B located at Brookhaven National Laboratory (NSLS). A greatly simplified representation of the tomographic process is

shown in Figure 1. At this beam-line the full spectrum of X rays from the synchrotron is passed from the ring to a monochromator crystal located in the instrument hutch about 20 m from the ring. A Si (111) crystal was used to produce a highly collimated monochromatic 17 keV X ray beam. This beam is incident on the 3-mm-diameter cylindrical specimen, which was cored from a larger specimen that had been previously backfilled with epoxy resin. X rays transmitted by the specimen are converted to light using an optically polished CsI(Tl) crystal. Light emitted from the crystal is imaged onto the surface of a 512×512, 30 μm/pixel charge coupled device (CCD) using a 4 × numerical aperture = 0.2 microscope objective resulting in a 7.5 μm/pixel resolution radiograph of the specimen. For this configuration the resolution is limited by the CCD pixel size. A tomographic scan is accomplished by rotating the specimen about an axis perpendicular to the X ray beam and parallel to the CCD pixel columns while collecting radiographs of the specimen at small angular increments. A total of 720 radiographs of the specimen were collected at 0.25° angular increments between 0° and 180°.

Tomographic reconstruction is carried out by direct Fourier inversion [*Flannery et al.*, 1987]. X ray opacities (projections) are calculated from the radiographic data and are sorted by CCD pixel row to form the sinogram. The one-dimensional fast Fourier transform (FFT) of each row of the sinogram forms the two-dimensional Fourier transform of the projections in polar coordinates. A change of coordinates from polar to Cartesian is made using a weighted interpolation process. This is followed by an inverse two-dimensional FFT to reconstruct the slice. Since the synchrotron radiation is highly collimated, the same reconstruction algorithm is appropriate for each row of CCD pixels, as the CCD is a contiguous stack of 512 linear computerized tomography (CT) detector arrays operating in parallel. Three dimensional volumes are constructed by stacking the reconstructed slices. For our cylindrical specimens, this results in a $512 \times 512 \times 512$ cube of data with rock data in the inscribed 512-pixel-diameter cylinder. Data acquisition time for these specimens is about 1 hour. Data reconstruction requires an additional hour.

Data Segmenting

A tomographic image slice consists of a rectangular array of X ray attenuation coefficients, each associated with a finite-volume cube (voxel) of the sample. The attenuation coefficients are a function of the average density and composition of the material in any given voxel. This makes interpretation of the attenuation coefficients somewhat ambiguous. Therefore a plot of the attenuation coefficients is a measure of the density variation throughout the sample. Because of various aspects of X ray tomography, distinguishing between the grain and pore phases is not sharp. Therefore the attenuation histogram for a typical binary material consists of an overlapping bivariate distribution as illustrated in Figure 2. The peak at higher attenuation coefficients is associated with the grain phase. The large peak at lower attenuation values is associated with the external air space surrounding the sample. The middle peak arises from the epoxy filled pore space in the sandstone sample. It is the epoxy phase that we identify as the pore space in the sample.

For our quantitative analysis of the tomographic images, it is necessary to have a well-defined, self-consistent method of identifying each voxel as either pore or grain. Some traditional approaches involve choosing a threshold or cut-off attenuation coefficient value lying somewhere between the peaks in Figure 2; any voxel with attenuation coefficient value greater than the cut-off is identified as material while those with lower values are identified as pore. In general, choice of this cut-off is arbitrary and may not be the best approach for phase identification. It was recently demonstrated by *Jain and Dubuisson* [1992] that thresholding methods are inadequate for segmenting images with overlapping bivariate distributions that arise from X ray and CAT scan images. Their study included simple thresholding, adaptive thresholding, and iterated conditional modes. They argue that the inherent structure of an image can be better characterized through detec-

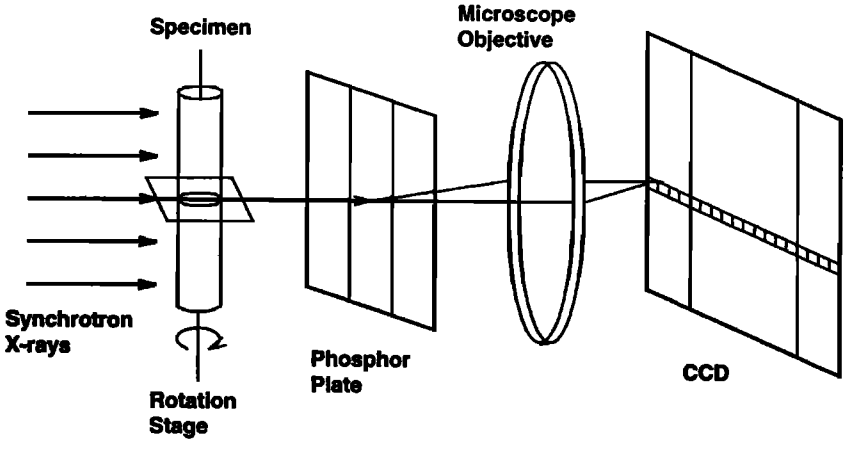

Figure 1. A simplified illustration of the X ray tomography imaging process.

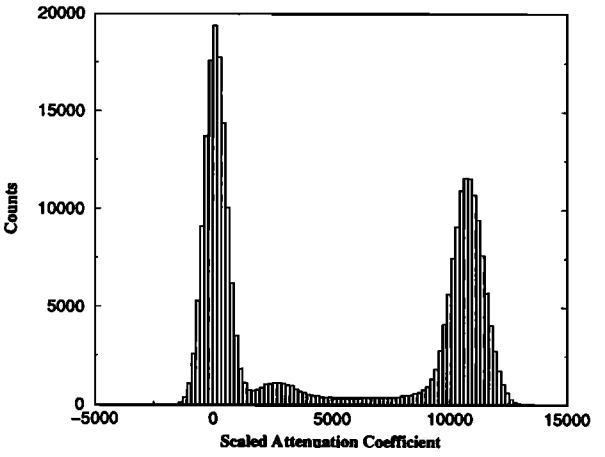

Figure 2. Example attenuation coefficient histogram (unfiltered) for Fontainebleau sandstone. The peak associated with large attenuation coefficients corresponds to the grain phase. The largest peak, associated with low attenuation values corresponds to the air surrounding the sample. The middle peak arises from the epoxy-filled pore space in the sandstone sample. The epoxy phase is identified as the pore space in the sample.

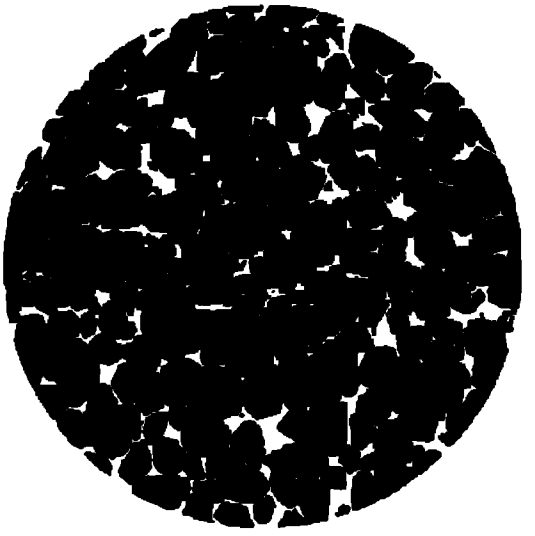

Figure 3. Sample filtered slice of Fontainebleau sandstone. The black region corresponds to the grain phase. The diameter of the cylindrical core is 3 mm with a voxel resolution of 7.5 μm

tion and localization of the edges separating the various phases. These conclusions are further supported by the literature [*Beghdadi and Negrate,* 1989; *Leu,* 1992]. Therefore, we use an edge-based segmentation algorithm [*Coker and Lindquist,* 1994] that is a compromise between a simple threshold approach and the algorithmic complications associated with these published edge-enhancing segmentation algorithms. As tomographic images are obtained slice-wise, with consequent potential normalization deviations between different slices, our segmenting procedure is performed on individual slices. A sample filtered slice is shown in Figure 3.

Definition of Morphological Quantities and Corresponding Bounds

In the most general situation the random medium is a domain of space $V(\omega) \in \mathcal{R}^3$, where the realization ω is taken from some probability space of volume V, which is composed of two regions or phases: phase 1 region (the void phase) $\mathcal{V}_1$ of volume fraction ϕ_1 and phase 2 region (the grain phase) $\mathcal{V}_2$ of volume fraction ϕ_2. Let $\partial\mathcal{V}$ denote the surface or interface between $\mathcal{V}_1$ and $\mathcal{V}_2$. For a given realization ω the characteristic function $\mathcal{I}(\mathbf{x})$ of phase 1 is given by

$$\mathcal{I}(\mathbf{x}) = \begin{cases} 1 & \mathbf{x} \in \mathcal{V}_1 \\ 0 & \mathbf{x} \in \mathcal{V}_2. \end{cases} \tag{1}$$

The characteristic function $\mathcal{M}(\mathbf{x})$ for the interface is defined as

$$\mathcal{M}(\mathbf{x}) = |\nabla\mathcal{I}(\mathbf{x})|. \tag{2}$$

This notation translates into a designation of each phase of the tomographic image with a value of 0 or 1. In this investigation we associate a value of 1 with the grain phase and a value of 0 with the pore phase. As this study concentrates on only one sample, there is only one realization ω, but the size of the sample is sufficiently large as to allow us to replace ensemble averaging with volume averaging.

The n–Point Probability Functions and Bulk Properties

The simplest morphological measures are the one-point correlation functions such as the volume fraction ϕ_i of phase i and the specific surface area s, both of which are defined in terms of the appropriate characteristic functions as

$$\phi_1 = 1 - \phi_2 = \langle\mathcal{I}(\mathbf{x})\rangle, \quad s = \langle\mathcal{M}(\mathbf{x})\rangle. \tag{3}$$

Here angular brackets denote ensemble averaging. Under the ergodic hypothesis, ensemble averaging can be replaced with volume averaging. The volume fraction ϕ_i has a simple probabilistic interpretation; it is the probability of finding a point in phase i.

The probability that two points separated by $\mathbf{r}$ both lie in the pore phase is denoted by $S_2(\mathbf{r})$. For isotropic media, the two-point probability function depends only on the magnitude of the separation r and is given by

$$S_2(r) = \langle\mathcal{I}(\mathbf{x}_1)\mathcal{I}(\mathbf{x}_1 + \mathbf{r})\rangle \tag{4}$$

where $r = \|\mathbf{r}\|$. Some important properties of $S_2(r)$ are

$$\begin{aligned} S_2(0) &= \phi_1 \\ \lim_{r\to\infty} S_2(r) &= \phi_1^2 \\ \frac{d}{dr}S_2(r)\,|_{r=0} &= -\frac{1}{4}s. \end{aligned} \tag{5}$$

More generally, the material's microstructure can be characterized by the n-point probability functions, S_n. $S_n(\mathbf{x}_1, \mathbf{x}_2, \ldots, \mathbf{x}_n)$ gives the probability of finding n points in the same phase at the positions, $\mathbf{x}_1, \ldots, \mathbf{x}_n$. There are several other n-point correlation functions and we refer readers to [*Torquato*, 1991] for a thorough review.

The n-point probability functions provide a useful probe with which to define several length scales characteristic of the sample. *Beran* [1968] mentions a characteristic length scale λ_A in terms of $S_2(r)$ as follows

$$\lambda_A = \int_0^\infty [S_2(r) - \phi_1^2]\, dr. \tag{6}$$

A length scale λ_B that appears in rigorous bounds on the fluid permeability [*Prager*, 1961;*Prager*, 1969] and trapping rate (or equivalently, mean survival time) [*Rubinstein and Torquato*, 1988] is defined by

$$\lambda_B = \left\{ \int_0^\infty [S_2(r) - \phi_1^2]\, r dr \right\}^{1/2}. \tag{7}$$

Prager [1961] first derived an upper bound on the fluid permeability k using λ_B that was corrected later by *Berryman and Milton* [1985] as

$$k \leq \frac{2\lambda_B^2}{3(1-\phi_1)^2}. \tag{8}$$

There exist sharper variational bounds on k that also depend on higher-order n-point quantities [*Torquato*, 1991].

Another length scale obtainable from the two-point function is its correlation length as defined by the distance at which the two-point function dwindles to its asymptotic value of ϕ_1^2; this scale will be referred to as λ_C.

An additional geometric parameter that plays an important role in determining the effective conductivity and the bulk modulus of a random medium is ζ_2 [*Torquato*, 1991]. This parameter lies in the range [0,1] and involves a multi-dimensional integral over the three-point probability function $S_3(y, z, \theta)$ [*Torquato*, 1980; *Milton*, 1981]. In three dimensions, ζ_2 is defined as follows:

$$\zeta_2 = 1 - \frac{9}{2\phi_1\phi_2} \int_0^\infty \frac{dz}{z} \int_0^\infty \frac{dy}{y} \int_{-1}^1 d(\cos\theta) \times P_2(\cos\theta) \left[S_3(y, z, \theta) - \frac{S_2(y) S_2(z)}{\phi_1} \right] \tag{9}$$

where $P_2(\cos\theta) = \frac{1}{2}[3\cos^2\theta - 1]$ is the second-order Legendre polynomial. As the three-point probability function $S_3(y, z, \theta)$ defines the probability of finding three points in the pore phase, it may be determined from a two-dimensional image [*Berryman*, 1985] rather than a full three-dimensional representation when the medium is isotropic.

Lineal Path and Chord Length Distribution Functions

Another important morphological descriptor is the lineal-path function $L(z)$ [*Lu and Torquato*, 1992a,b] which is the probability of finding a line segment of length z wholly in the void phase when thrown into a sample. A closely related quantity is the chord-length distribution function $p(z)$ [*Torquato and Lu*, 1993]. Specifically, $p(z)dz$ is the probability of a finding a chord of length between z and $z + dz$ in the void phase. Chords are distributions of lengths between intersections of lines with the two-phase interface. The first moment of $p(z)$, λ_D, mean chord length is defined as

$$\lambda_D = \int_0^\infty z p(z) dz. \tag{10}$$

Torquato and Lu [1993] showed that the lineal-path function and the chord-length distribution function for any statistically isotropic system are related according to the expression

$$p(z) = \frac{\lambda_D}{\phi_1} \frac{d^2 L(z)}{dz^2}. \tag{11}$$

Knowledge of $p(z)$ is of importance in transport problems involving "discrete free paths," such as Knudsen diffusion and radiative transport [*Ho and Streider*, 1979;*Tokunaga*, 1985].

Mean Survival Time, Pore Size Distribution, and Fluid Permeability

The mean survival time τ (obtainable from an nuclear magnetic resonance (NMR) experiment [*Banavar and Schwartz*, 1987; *Wilkinson et al.*, 1991; *Strange et al.*, 1993]) is the average time a Brownian or diffusing particle takes to diffuse in a trap-free region (with diffusion coefficient D) in a system of partially absorbing traps before becoming absorbed by the trapping phase. Therefore, the quantity $D\tau$ provides an average pore–size measure. In the Fontainebleau sandstone system, the void phase is identified with the trap-free region and the grain phase is identified with the trap region. The mean survival time is measured by simulating the Brownian motion of diffusing particles in the void phase. The time for each particle to diffuse to the void–grain boundary is measured for each particle and then averaged over all such particles. We use an efficient first-passage time algorithm first developed for continuum materials by *Torquato and Kim* [1989] and then later adapted to digitized media [*Coker and Torquato*, 1995a]. It was previously shown [*Coker and Torquato*, 1995a] that τ measured on a digitized medium provides a lower bound on the true continuum mean survival time.

The pore–size distribution function $P(\delta)$ [*Scheidegger*, 1974; *Torquato and Avellaneda*, 1991], is defined such that $P(\delta)d\delta$ is the probability that a randomly chosen location in the pore phase lies a distance between δ and $\delta + d\delta$ of the nearest point on the pore–solid interface. It is important to note that $P(\delta)d\delta$ can be

obtained only from a three-dimensional representation of the sample, as it contains some connectedness information about the pore space [*Torquato*, 1994]. $P(\delta)$ satisfies the following properties

$$\int_0^\infty P(\delta)d\delta = 1, \quad P(\infty) = 0 \tag{12}$$

with

$$P(0) = \frac{s}{\phi_1}, \tag{13}$$

where s is the specific surface area as defined above. The mean pore size λ_E is defined by the first moment of $P(\delta)$, i.e.,

$$\lambda_E = \langle\delta\rangle = \int_0^\infty \delta P(\delta)d\delta. \tag{14}$$

The mean survival time τ has been rigorously bounded from below in terms of the mean pore size λ_E [*Torquato and Avellaneda*, 1991] via the relation

$$\tau \geq \lambda_E^2/D\,, \tag{15}$$

where D is the diffusion coefficient.

The cumulative distribution function $F(\delta)$ associated with $P(\delta)$ is defined by

$$F(\delta) = \int_\delta^\infty P(z)dz \tag{16}$$

with

$$F(0) = 1 \quad F(\infty) = 0. \tag{17}$$

$F(\delta)$ is the fraction of pore space that has a pore diameter greater than δ. The mean pore–size may also be defined in terms of the cumulative pore–size distribution function,

$$\lambda_E = \int_0^\infty F(\delta)d\delta. \tag{18}$$

Torquato [1991] developed a rigorous cross-property relation that relates the fluid permeability k to the mean survival time τ as follows:

$$k \leq \phi_1 D\tau\,. \tag{19}$$

Thus a measurement of the mean survival time provides an upper bound on the fluid permeability. Relation (19) becomes an equality for transport interior to parallel tubes of arbitrary cross-section (in the direction of the tubes). The bound (19) is relatively sharp for flow around dilute arrays of obstacles; for example, for spheres $k = 2D\phi_1\tau/3$. For a cubic array of narrow tubes it is less sharp: $k = D\phi_1\tau/3$. Generally, inequality (19) is not sharp because τ is a reflection of the entire pore space, whereas k is a reflection of the dynamically connected part of the pore space.

Avellaneda and Torquato [1991] derived the first rigorous equality connecting the permeability to the effective electrical conductivity σ_e of a porous medium containing a conducting fluid of conductivity σ_1 and an insulating solid phase:

$$k = \frac{L^2}{8\mathcal{F}}\,, \tag{20}$$

where $\mathcal{F} = \sigma_1/\sigma_e$ is the formation factor and L is a length parameter which is a weighted sum over the viscous relaxation times associated with the time-dependent Stokes equations.

Since it is difficult to obtain L^2 exactly, rigorous treatments can only provide bounds on L^2. It has been conjectured [*Torquato and Kim*, 1992] that for isotropic media possessing an arbitrary but connected pore space, the following relation holds:

$$k \leq \frac{D\tau}{\mathcal{F}}\,. \tag{21}$$

Because the right-hand side of (21) appears to overestimate k by roughly a factor of porosity ϕ_1 for a number of porous media, it has been proposed [*Schwartz et al.*, 1993] that the approximate relation

$$k \approx \phi_1 \frac{D\tau}{\mathcal{F}}\,, \tag{22}$$

should be accurate for a large class of porous media. This relation will be tested in the subsequent section.

It should be noted that the approximate formula

$$k = \frac{\Lambda^2}{8\mathcal{F}}\,, \tag{23}$$

developed by *Johnson et al.* [1986] provides a good estimate of k for a variety of media. Here Λ^2 is a dynamically weighted ratio of pore volume to surface area that involves the electric field. It is not as easy to measure directly as either $\mathcal{F}$ or τ, however.

Coarseness

A quantity that has many implications in the investigation of microstructure for real materials is the coarseness, C, first studied by *Lu and Torquato* [1990]. This quantity provides a quantitative measure of local porosity fluctuations and hence of the uniformity of the coverage of the phases. The standard deviation associated with the characteristic function σ_I for an infinite system is a constant that does not provide much useful structural information about the random medium. In particular, σ_I for fluctuations associated with the volume fraction of the void phase, is given by

$$\frac{\sigma_I}{\phi_1} = \frac{\langle\mathcal{I}^2\rangle - \langle\mathcal{I}\rangle^2}{\phi_1} = \frac{\phi_1 - \phi_1^2}{\phi_1}. \tag{24}$$

In contrast, the coarseness is given in terms of the stochastic quantity, $\tau(\mathbf{x})$ which is the local volume fraction of the void phase measured in a window of finite size V_0 at $\mathbf{x}$ with $\langle\tau(\mathbf{x})\rangle = \phi_1$. Thus the coarseness is given by

$$C = \frac{\sigma_\tau}{\phi_1} \tag{25}$$

where σ_τ is the standard deviation associated with measuring τ. As a consequence of its definition, C is dependent on the volume and shape of the observation

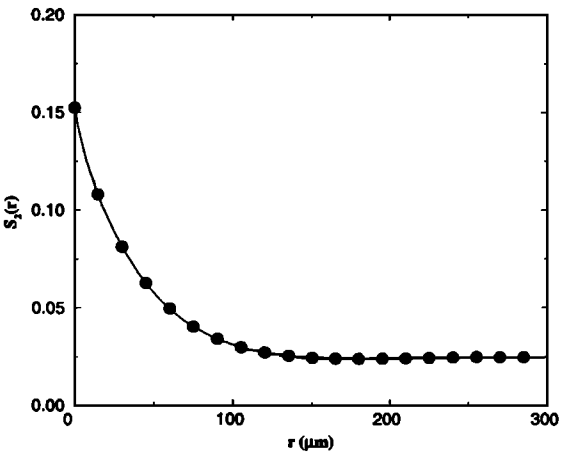

Figure 4. Two-point probability function for Fontainebleau sandstone.

window and reduces to σ_I/ϕ_1 in the limit $V_0 \to \infty$. It was also shown that C can be related to the two-point probability function described earlier [*Lu and Torquato,* 1990].

Morphological Results and Predictions

In the results that follow, each voxel of the reconstructed tomographic image is a cubic region of size $7.5 \times 7.5 \times 7.5$ μm^3 and comprises a single phase, grain, or pore. Therefore the phase of a randomly chosen point is that of the voxel in which it resides. The algorithms for the previous study involving digitized spheres [*Coker and Torquato,* 1995a,b] were developed primarily for rectangular regions within a slice and a series of slices forming a rectangular volume. All two-dimensional quantities are computed within each slice, and the results are averaged across slices. Therefore we extract the largest possible rectangular volume from the center of the cylindrical drill core sample shown in Figure 3. The sample consisted of roughly 300 planar slices separated by a distance of 7.5 μm. Because of various experimental difficulties, some internal slices had to be discarded, reducing the number of useful slices to 296.

As was discussed above, previous work [*Coker and Torquato,* 1995b] with overlapping digitized sphere systems showed that certain morphological quantities were highly sensitive to the digitized nature of the sample. In somewhat practical terms this translates into a resolution dependence. Therefore we will draw upon this experience to place the following results with the Fontainebleau specimen in a more informed context.

The one-point probability function ϕ_1 is found to be 0.154, which is in close agreement with the experimental measurement of 0.148 [*Schwartz et al.,* 1994] as discussed below.

The two-point probability function averaged across slices of the Fontainebleau specimen is given in Figure 4. The structure of this curve is reminiscent of materials composed of overlapping granules. As the two-point probability function is not very sensitive to the underlying morphology, this is not a surprising result. As was mentioned above, the two-point probability function may be used to define the length scales, λ_A, λ_B, and λ_C. These are given in Table 1. In earlier work [*Coker and Torquato,* 1995b], each of these quantities was found to be relatively insensitive to the digitization process. The uncertainties given in Table 1 measure the statistical fluctuations across slices and are not indicative of measurement error. Such large statistical fluctuations are therefore due to the limited size of each slice. The coarseness is given in Figure 5. Since C is computed in an observation volume having a thickness of one slice, it provides a useful measure of the statistical fluctuations one will encounter in going from slice to slice in a digitized medium. This volume V_O is scaled by the volume of a sphere with diameter λ_C. This is done because λ_C provides a convenient length scale beyond which correlations have died out. As can be seen in Figure 5, C at relatively large volumes is still approximately 0.14. Therefore, the size of the Fontainebleau specimen is statistically small, giving rise to the large fluctuations shown in Table 1.

In Table 2 the specific surface area s for the digitized specimen is given using two different methods: direct measurement and formula (5). The latter is one of the most common methods of extracting s and relies on the use of the two-point probability function $S_2(r)$. The direct measurement of the specific surface area is performed by counting the exposed surface area of each three-dimensional voxel belonging to the grain phase. The direct measurement is an exact measure of the digitized sample and provides an upper bound

Table 1. Characteristic Length Scales Studied in This Investigation

Parameter	Definition	Description	Measured Value
λ_A	$\int_0^\infty [S_2(r) - \phi_1^2]\, dr$	Mean Value of $(S_2 - \phi_1^2)$	4.6 ± 1.6 μm
λ_B^2	$\int_0^\infty r\,[S_2(r) - \phi_1^2]\, dr$	First Moment of $(S_2 - \phi_1^2)$	144.0 ± 24 μm^2
λ_C	see text	correlation length	~ 200 μm
λ_D	$\int_0^\infty zp(z)dz$	mean chord length	44.5 ± 5 μm
λ_E	$\int_0^\infty \delta P(\delta)d\delta$	mean pore size	10.2 ± 0.1 μm
ζ_2	Equation (9)	three-point parameter	0.42 ± 0.16
τD	see text	survival time × diffusion coefficient	154 ± 6 μm^2

The last column includes the measured values as discussed in the text. In addition, this table contains the resulting measurement of ζ_2.

on the true specific surface area. The specific surface area obtained from $S_2(r)$ is shown in Table 2 for several different resolutions. The lower-resolution results will be more consistent with the continuum or experimental result, while the higher-resolution results will approach the direct result. This phenomenon is clearly seen in Table 2. Obtaining an exact measurement of the continuum specific area is difficult because of this resolution dependence. However, it was shown [*Coker and Torquato,* 1995b] that a medium-resolution (1/2 – 1 voxel) gives a result that closely approximates that of the continuum system. In fact, the lower-resolution measurements indeed provide a value much closer to the experimental value (see Table 2) than the direct method. In the infinite resolution limit, the direct result could be obtained from the use of (5).

The void lineal-path function $L(z)$ and the chord-length distribution function $p(z)$ are shown in Figure 6. Owing to the digitized nature of the specimen and the sensitivity of $p(z)$ to the grain-void interface, the first moment, λ_D is probably somewhat smaller than the actual value. Given the pore volume fraction, we estimate that it is approximately 5% less than the actual value.

As was mentioned above, $P(\delta)$ and $F(\delta)$ are intrinsically three-dimensional quantities. These quantities were measured on sample volumes of dimension 2250 × 2250 × 1583 μm^3. This volume is equivalent to 211 slices which is less than the 296 slices discussed above because various neighboring slices were missing as a result of experimental difficulties. The results are shown in Figure 7. The mean pore-size is shown in Table 1. Previous work on overlapping digitized sphere systems demonstrated that digitized systems contained larger numbers of small pores and consequently fewer numbers of large pores. Therefore the measured mean pore-size is diminished possibly by as much as 20% depending on the exact geometry of the pore-grain interface.

Let us now consider the effective properties of the Fontainebleau data set. The mean survival time τ was directly determined from the data set using the first-passage time algorithm for digitized media discussed earlier [*Coker and Torquato,* 1995a]. Table 1 shows that τD is equal to 154 μm^2. It is interesting to compare this value to the rigorous lower bound (15). From the value of λ_E given in Table 1, it is found that τD must be greater than 104 μm^2, and thus this bound (15) is relatively sharp.

The parameter $\zeta_2 = 0.42$ (see Table 1), which determines bounds on the effective conductivity [*Torquato,* 1980; *Milton,* 1981] and elastic moduli [*Milton,* 1981], was determined using a previously developed algorithm [*Coker and Torquato,* 1995b]. The large uncertainty in ζ_2 arises from the relatively small sample size available. The three-point probability function that arises in the integrand of ζ_2 does not decay fast enough for the sample sizes studied here, leading to nonzero contributions that cannot be accurately accounted for. This information is utilized to compute a rigorous upper bound on the dimensionless effective conductivity when the pore fluid has a conductivity σ_1 and a nonconducting

Table 2. Specific Surface Area s

Resolution	s, 10^4 m^{-1}
Direct	2.08
1/6	1.68
1/3	1.63
1/2	1.58
2/3	1.54
5/6	1.50
1	1.43
Experimental	1.54

"Direct" refers to a voxel-by-voxel counting of surface area, while "1", "1/3", etc., determine the spacing in terms of voxels used to compute the derivative to obtain s using equation (5). The uncertainty for the results obtained here is approximately 15% because of the limited sample size. The experimental value is given by *Schwartz et al.* [1994].

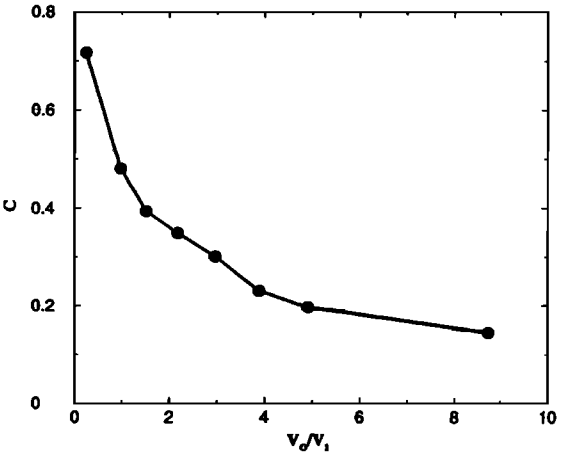

Figure 5. Coarseness, C, as a function of scaled observation window for Fontainebleau sandstone. V_1 is the volume of a sphere with diameter λ_C and V_O is the volume of the observation window.

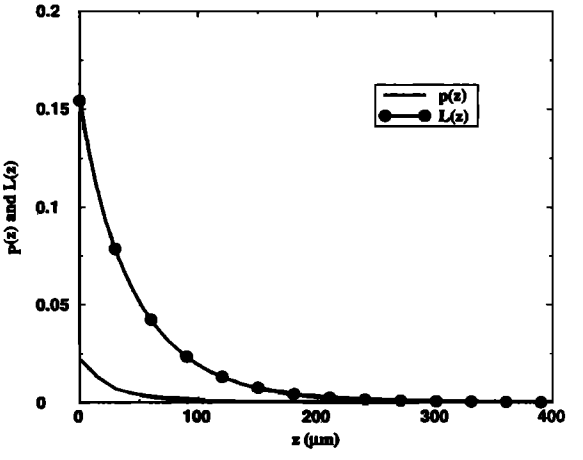

Figure 6. Pore chord-length distribution function $p(z)$ and lineal-path function $L(z)$ for Fontainebleau sandstone. The chord-length distribution function is shown in units of probability density while the lineal-path function is shown in units of probability.

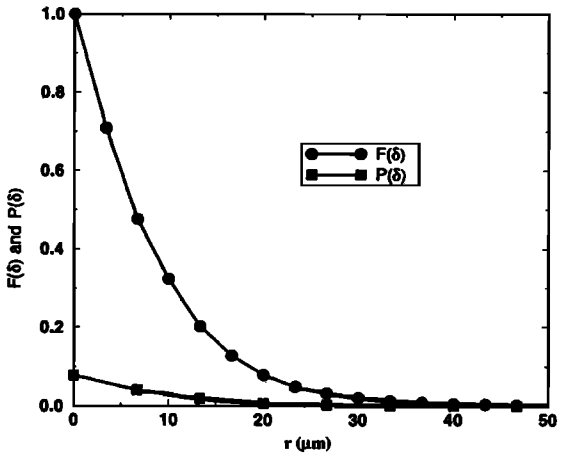

Figure 7. Pore-size distribution function $P(\delta)$ and the cumulative pore-size distribution function $F(\delta)$ for Fontainebleau sandstone. The pore-size distribution function is shown in units of probability density while the cumulative pore-size distribution function is shown in units of probability.

grain phase,that is, $\sigma_e/\sigma_1 = \mathcal{F}^{-1} \leq 0.089$. This is to be contrasted with the experimentally measured values [*Schwartz et al.*, 1994] of $\sigma_e/\sigma_1 = \mathcal{F}^{-1} = 0.0265$. Thus the bound is not as sharp here as in the case of the mean survival time.

Consider now the predictions of the permeability k. Experimentally, it was found that $k = 1.3\ \mu\text{m}^2$ [*Schwartz et al.*, 1994]. Using λ_B in Table 1 and our measured porosity $\phi_1 = 0.154$, bound (8) reads

$$k \leq 134\ \mu\text{m}^2\ . \tag{26}$$

This is obviously a weak bound. Employing τ of Table 1 and our measured porosity $\phi_1 = 0.154$, bound (19) reads

$$k \leq 23.7\ \mu\text{m}^2\ . \tag{27}$$

Utilizing Table 1 and the rigorous upper bound $\sigma_e/\sigma_1 = \mathcal{F}^{-1} =\leq 0.089$ described immediately above, bound (21) reads

$$k \leq 13.7\ \mu\text{m}^2\ . \tag{28}$$

Note that a rigorous upper bound on $\mathcal{F}^{-1}$ maintains the inequality of bound (21). Finally, using τ from Table 1, the rigorous upper bound $\sigma_e/\sigma_1 = \mathcal{F}^{-1} =\leq 0.089$ and our measured porosity $\phi_1 = 0.154$, approximation (22) reads

$$k \approx 2.1\ \mu\text{m}^2\ . \tag{29}$$

Clearly, formula (29) provides an accurate and the best estimate of the permeability. Although it is not a rigorous upper bound, it turns out to bound the measured value from above.

Concluding Remarks

We conducted a statistical analysis on a high-resolution, three-dimensional, tomographic representation of a piece of Fontainebleau sandstone. We determined the two-point probability function, ζ-parameter, lineal path function, chord-length distribution function, pore-size distribution function, and coarseness. Determination of the pore-size distribution could not have been done without such a data set, since it is an intrinsically three-dimensional measure that cannot be obtained from a two-dimensional image. Determination of these statistical quantities allowed us to predict effective properties of real materials such as mean survival time, permeability, and conductivity. The bound for the mean survival time was relatively sharp, the permeability was an upper bound within a factor of 1.6 of the experimental value, and the conductivity bound was about 3 times larger than the experimental value. As with any digitized representation of real materials, it is important to bear in mind that the digitization, finite resolution, and finite sample size may affect any measured quantity. Finite sample size results primarily in statistical uncertainties, while digitization and finite resolution result in quantitative shifts of the measured quantities.

Acknowledgments. D.A.C. and S.T. acknowledge the support of the Office of Basic Energy Science, U.S. Department of Energy, under grant DE-FG02-92ER14275 and the Petroleum Research Fund. D.A.C. also gratefully acknowledges the support of the San Diego Supercomputer Center for the development of the parallel version of the algorithms used in this study. J.D. gratefully acknowledges the support of Exxon Research and Engineering Co. We would also like to thank both Exxon Research and Engineering Company and L.M. Schwartz for use of the Fontainebleau tomographic data set.

References

Avellaneda, M., and S. Torquato, Rigorous link between fluid permeability, electrical conductivity, and relaxation times for transport in porous media, *Phys. Fluids A, 3*, 2529, 1991.

Banavar, J.R., and L.M. Schwartz, Magnetic resonance as a probe of permeability in porous media, *Phys. Rev. Lett, 58*, 1411, 1987.

Beghdadi, A., and A.L. Negrate, Contrast enhancement technique based on local detection of edges, *Comput. Vision Graphics Image Process., 46*, 162, 1989.

Beran, M. J., *Statistical Continuum Theories*, 424 pp., John Wiley, New York, 1968.

Berryman, J. G., Measurement of spatial correlation functions using image processing techniques, *J. Appl. Phys. 57*, 2374, 1985.

Berryman, J. G., and S. Blair, Use of digital image analysis to estimate fluid permeability of porous materials: Application of two-point correlation functions, *J. Appl. Phys., 60*, 1930, 1986.

Berryman, J. G., and G.W. Milton, Bounds on fluid permeability for viscous flow through porous media, *J. Chem. Phys., 83*, 754, 1985.

Coker, D. A., and W.B. Lindquist, Edge-based algorithm to filter tomographic data sets, *SUNYIT-MS-1-1994*, Dept. of Math. and Sci., State Univ. of N. Y. Inst. of Technol., Utica, N.Y., 1994.

Coker, D.A. and S. Torquato, Simulation of diffusion and trapping in heterogeneous random media, *J. Appl. Phys., 77*, 955, 1995a.

Coker, D.A. and S. Torquato, Extraction of morphological quantities from a digitized medium, *J. Appl. Phys., 77*, 6087, 1995b.

Darcy, H.P.G., *Les fontaines publiques de la Ville de Dijon*, Victor Dalmont, Paris, 1856.

Deckman, H.W., K.L. D'Amico, J.H. Dunsmuir, B.P. Flannery, and S.M. Gruner, Microtomography detector design: it's not just resolution, *Adv. in X Ray Anal. 32*, 641, 1989.

Doi, M., A new variational approach to the diffusion and flow problem in porous media, *J. Phys. Soc. Japan. 40*, 567, 1976.

Dullien, F.A.L., *Porous Media - Fluid Transport and Pore Structure*, Academic, San Diego, Calif., 1979.

Dunsmuir, J.H., S.R. Ferguson, and K.L. D'Amico, Design and operation of an imaging X-ray detector for microtomography, paper presented at conference on Photoelectric Image Devices, Institute for Physics, London, Sept. 1991.

Flannery, B. P., H. W. Deckman, W. G. Roberge, and K. L. D'Amico, Three dimensional x-ray microtomography, *Science, 237*, 1439, 1987.

Flegler, S. L., *Scanning and Transmission Electron Microscopy: An Introduction*, 225 pp., W.H. Freeman, New York, 1993.

Fredrich, J. T., B. Menendez, and T.F. Wong, Imaging the pore structure of geomaterials, *Science, 268*, 276, 1995.

Ho, F. G., and W. Strieder, Aysmptotic exapansion of the porous medium, effective diffusion coefficient in the Knudsen number, *J. Chem. Phys., 70*, 5635, 1979.

Jain, A. K., and M.-P. Dubuisson, Segmentation of x-ray and c-scan images of fiber reinforced composite materials, *Pattern Recognition, 25*, 257, 1992.

Johnson, D. L., J. Koplik, and L.M. Schwartz, New pore-size parameter characterizing transport in porous media, *Phys. Rev. Lett, 57*, 2564, 1986.

Kinney, J. H., and M. C. Nichols, X-ray tomographic microscopy (XTM) using synchrotron radiation, *Annu. Rev. Mater. Sci., 22*, 121, 1992.

Kwiecien, M. J., I. F. MacDonald, and F. A. L. Dullien, Three-dimensional reconstruction of porous media from serial section data, *J. Microsc., 159*, 343, 1990.

Leu, J.-G., Image contrast enhancement based on the intensities of edge pixels, *CVGIP Graphical Models Image Process., 54*, 497, 1992.

Lu, B., and S. Torquato, Local volume fraction fluctuations in heterogeneous media, *J. Chem. Phys., 93*, 3452, 1990.

Lu, B., and S. Torquato, Lineal path function for random heterogeneous materials, *Phys. Rev. A, 45*, 922, 1992a.

Lu, B., and S. Torquato, Lineal path function for random heterogeneous materials II. Effect of Polydispersivity, *Phys. Rev. A, 45*, 7292, 1992b.

MacDonald, I. F., P.M. Kaufmann, and F.A.L. Dullien, Quantitative image analysis of finite porous media I. Development of genus and pore map software, *J. Microsc., 144*, 277, 1986.

Milton, G. W., Bounds on the electromagnetic, elastic, and other properties of two–component composites, *Phys. Rev. Lett, 46*, 542, 1981.

Milton, G.W., Multicomponent composites, electrical networks and new types of continued fraction I, *Commun. Math. Phys., 111*, 281, 1987.

Prager, S., Viscous flow through porous media, *Phys. Fluids, 4*, 1477, 1961.

Prager, S., Viscous flow through porous media, *J. Chem. Phy., 50*, 4305 1969.

Rubinstein, J., and S. Torquato, Diffusion-controlled reactions: Mathematical formulation, variational principles, and rigorous bounds, *J. Chem. Phys., 88* , 6372, 1988.

Rubinstein, J., and S. Torquato, Flow in random porous media: Mathematical formulation, variational principles and rigorous bounds, *J. Fluid Mech., 206*, 25, 1989.

Scheidegger, A. E., *The Physics of Flow Through Porous Media*, 353 pp., Univ. of Toronto, Toronto, Ont., Canada, 1974.

Schwartz, L.M., N. Martys, D.P. Bentz, E.J. Garboczi, and S. Torquato, Cross-property relations and permeability estimation in model porous media, *Phys. Rev. E Stat. Phys. Plasmas Fluids Relat.Interdiscp.Top.*, 48, 4584, 1993.

Schwartz, L.M., F. Auzerais, J. Dunsmuir, N. Martys, D.P. Bentz, and S. Torquato, Transport and diffusion in three dimensional composite media, *Physica, A 207*, 28, 1994.

Strange, J.H., M. Rahman, and E.G. Smith, Characterization of porous solids by NMR, *Phys. Rev. Lett, 71*, 3589, 1993.

Stroscio, J. A., and W. J. Kaiser (Eds.), *Scanning Tunneling Microscopy*, 459 pp., Academic,San Diego, Calif., 1992.

Tokunaga, T. K., Porous media gas diffusivity from a free path distribution model, *J. Chem. Phys., 82*, 5298, 1985.

Torquato, S., Microscopic approach to transport in two-phase random media, Ph.D. thesis, State Univ. of New York at Stony Brook, Stony Brook, 1980.

Torquato, S., Microstructure characterization and bulk properties of disordered two-phase media, *J. Stat. Phys., 45*, 843, 1986.

Torquato, S., Relationship between permeability and diffusion-controlled trapping constant of porous media, *Phys. Rev. Lett, 64*, 2644, 1990.

Torquato, S., Random heterogeneous media: Microstructure and improved bounds on effective properties, *Appl. Mech. Rev., 44*, 37, 1991.

Torquato, S., Unified methodology to quantify the morphology and properties of inhomogeneous media, *Physica A 207*, 79, 1994.

Torquato, S., and M. Avellaneda, Diffusion and reaction in heterogeneous media: Pore size distribution, relaxation times, and mean survival time, *J. Chem. Phys., 95*, 6477, 1991.

Torquato, S., and I.C. Kim, An Efficient simulation technique to compute effective properties of heterogeneous media, *Appl. Phys. Lett., 55*, 1847, 1989.

Torquato, S., and I.C. Kim, Cross-property relations for momentum and diffusional transport in porous media, *J. Appl. Phys., 72*, 2612, 1992.

Torquato, S., and B. Lu, Chord-length distribution function for two-phase random media, *Phys. Rev., E 47*, 2950, 1993.

Underwood, E. E., *Quantitative Stereology*, Addison-Wesley, Reading, Mass., 1970.

Wilkinson, D.J., D.L. Johnson, and L.M. Schwartz, Nuclear magnetic relaxation in porous media: The role of the mean lifetime, *Phys. Rev. B, Condens. Matter, 44*, 4960, 1991.

D.A. Coker, Department of Mathematics and Science, State University of New York Institute of Technology, Utica, NY 13504-3050; (315) 792-7397 (phone), (315) 792-7503 (fax). (e-mail: coker@astro.sunyit.edu)

J.H. Dunsmuir, Exxon Research & Engineering Co. US Route 22 East, Annandale, NJ 08801 (908) 730-2548 (phone), (908) 730-3042 (fax). (e-mail: jh dunsm@erenj.com)

S. Torquato (corresponding author), Department of Civil Engineering and Operations Research, and Princeton Materials Institute, Princeton University, Princeton, NJ 08544, (609) 258-3341 (phone), (609) 258-2685 (fax). (e-mail: torquato@matter.princeton.edu)

(Received June 29, 1995; revised February 26, 1996; accepted March 6, 1996.)